Measurements and quality assessments of near-infrared plasma glucose spectra in the combination band region using a scanning filter spectrometer

Vidi Saptari
Delta Search Labs
400 Technology Square
Cambridge, Massachusetts 01239

Kamal Youcef-Toumi
MIT
77 Massachusetts Avenue
Cambridge, Massachusetts 02139

Abstract. Near-infrared measurements of glucose in human plasma are performed using a custom, rapid, high-throughput filter-based spectrometer covering a spectral range between 2080 and 2315 nm. Quality of the measured glucose signals is quantified through the use of two figures of merit: selectivity and limit of detection. Selectivity measures the uniqueness of the glucose spectrum from among the interfering spectra. Limit of detection measures the smallest glucose concentration change detectable. The proposed system, which includes the spectroscopic hardware and a spectral preprocessing algorithm, is shown to produce a selectivity value of 0.57, with zero being nonselective and one being fully selective, and a limit of detection value of 2.2 mM. Prediction of an independent dataset is also performed using net analyte signal-based and partial least-squares multivariate calibration techniques, which produce standard error of prediction values of 1.14 and 1.45 mM, respectively. [DOI: 10.1117/1.2141934]

Keywords: noninvasive; diabetes; spectroscopy; sensitivity; selectivity.

Paper 04133RR received Jul. 13, 2004; revised manuscript received Jun. 19, 2005; accepted for publication Jun. 20, 2005; published online Dec. 29, 2005.

1 Introduction

Research in the area of noninvasive blood glucose sensing using near-infrared (NIR) spectroscopy has been ceaseless in the last few decades. The degrees of success reported have been mixed, and a clinically accurate and reliable system has yet to be developed. The nature of empirical-based data processing algorithms generally used in this field makes it difficult to determine the quality of a glucose-specific signal actually present in the measured spectral data. This has, to some extent, prevented maximum progress, as knowledge transfer is difficult. Reasons for success (or failure) of the experimental works reported are often not clearly known. Thus, similar mistakes may have often been repeated, and improvements cannot be logically thought up.

Furthermore, most research efforts have been focused on the software component, specifically on improving the accuracy and reliability of multivariate calibration models.[1–8] As important as they are, the spectroscopic hardware that produces the raw spectral data should not be neglected. It is well known that clinically relevant blood glucose variations produce extremely small spectral changes. For clinically accurate readings, a signal-to-noise ratio of the order of at least 10^5 is needed, a stringent requirement for any spectroscopic instrument.[9]

In this work, we briefly describe a unique scanning NIR spectrometer that is designed specifically for blood glucose measurements. The main design criteria are high throughput and rapid scanning capability to maximize the signal-to-noise ratio. Undemanding resolution and bandwidth requirements enable us to satisfy these criteria with a simple and low-cost filter-based instrument.

Methods are presented that evaluate easily and objectively the quality of measured spectra. This is done by introducing two figures of merit that quantify selectivity (SEL) of glucose NIR signals in a certain background solution (matrix) and the resulting limit of detection (LOD). This way, success of the experimental work can be measured by a consistent and more objective means. Until now, it has generally been gauged by the standard error of prediction (SEP) of a prediction plot alone, whose values depend on many experimental and computation parameters, and requires the completion of a relatively large-scale experiment.

2 Spectroscopic Hardware

The spectrometer used in this work is a modified version of a previously reported rotating-filter spectrometer.[9] In this instrument, a second narrowband interference filter is added to cover the full available spectral window in the combination band region, approximately between 2080 and 2315 nm. Note that this window is mainly determined by the absorption spectrum of water,[10] the main component of tissue and blood. Figure 1 shows the optical layout of the spectrometer. One of the filters (model NB2210-010-B, Spectrogon, Parsippany, New Jersey) covers a spectral range approximately between 2080 and 2210 nm, and the other (model NB2310-010-B, Spectrogon) covers ~2200 through ~2315 nm. The former

Address all correspondence to Vidi Saptari, E-mail: vidi@alum.mit.edu

1083-3668/2005/10(6)/064039/9/$22.00 © 2005 SPIE

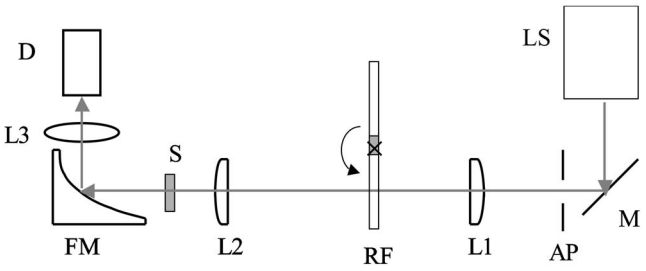

Fig. 1 A simplified optical layout of the spectrometer containing a light source (LS), a plane mirror (M), a circular aperture (AP), collimating and focusing CaF_2 lenses (L1, L2, and L3), the rotating filter assembly (RF), a parabolic focusing mirror (FM), and a detector (D). The sample (S) is placed between L2 and FM.

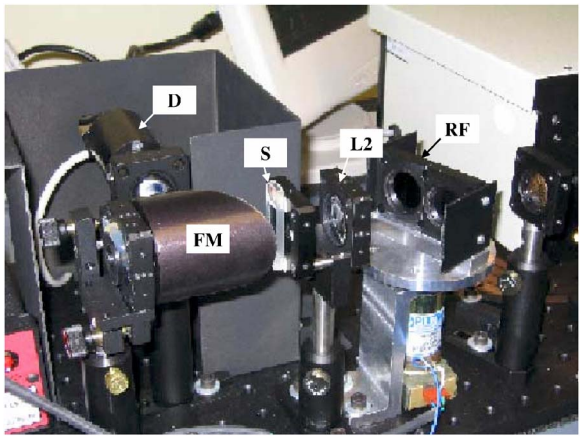

Fig. 2 A photograph of the rotating filter assembly.

has a nominal center wavelength (the center wavelength at zero degree incident angle) at 2210 nm, and the latter at 2310 nm. Both filters have 10-nm nominal FWHH bandwidths and transmittance peaks larger than 50% according to the manufacturer's specification.

Wavelength tuning is accomplished by rotating the filters in the direction shown in the diagram, through which the beam incident angle is varied. The peak transmission wavelength is a function of the beam incident angle λ_T, and can be described by the following equation:

$$\lambda_T = \lambda_0 \left[1 - \left(\frac{n_0}{n_{\text{eff}}} \right)^2 \sin^2 \varphi \right]^{1/2}, \qquad (1)$$

where λ_0 is the wavelength at a normal incident angle, n_0 is the refractive index of the external medium, n_{eff} is the refractive index of the filter, and φ is the incident angle.

The light source is a 250-W tungsten halogen (model LSH-T250, Jobin Yvon, Edison, New Jersey) powered by a DC-stabilized power source (model LPS250, Jobin Yvon). The detector is a two-stage thermoelectrically cooled extended InGaAs (model IGA2.2-010-TE2-H, Electro-Optical Systems, Phoenixville, Pennsylvania), operating at −30 °C. Calcium fluoride lenses are used to provide high transmittance throughout the combination band region.

A low-cost brush DC motor (model 8324S005, Pittman, Harleysville, Pennsylvania) rotates the filter assembly continuously counterclockwise (when viewed from above) at a speed of approximately 400 rpm. A picture of the assembly is shown in Fig. 2. No velocity feedback control is employed (the motor is run in an "open-loop" configuration).

In each revolution, there are two useful "windows" for each filter: 0 to 45 deg and 325 to 360 deg. Only one window is used at this time for ease of data processing, resulting in 6.7 scans per second or 400 scans per minute. Currently, the motor speed is limited by the bearing assembly, which is nonoptimal, as the bearing within the small motor assembly carries all of the dynamic load. Design improvements of the bearing assembly would easily enable a rotational speed on the order of 6000 rpm, resulting in 6000 scans per minute.

The motor unit has an integrated optical encoder providing 500 pulses per revolution and an index pulse once per revolution. The encoder pulses are used to "clock" the data acquisition (signal is captured at each pulse occurrence), while the index pulse is used to start or trigger it. The routine is programmed on a 16-bit data acquisition PCI board (model PCI-6032E, National Instruments, Texas). The raw data are transferred to Matlab for further processing. Since data acquisition is clocked by pulses whose timing directly corresponds to the incident angle φ, accuracy of the acquired data is insensitive to potential velocity errors. Thus, a velocity feedback control is not necessary, simplifying the associated electronics.

Since the transmitted wavelength is not a linear function of the incident angle [see Eq. (1)] while data is acquired at equal angular distance (once every 360/500 deg), the resulting spectral spacing is not constant. It varies from 0.04 nm at around 0 deg to 3.4 nm at around 45 deg. This would not pose any problem, however, as the resulting spectra can always be "linearized" to be presented just like spectra obtained from conventional spectrometers having constant spectral point spacing.

Such a spectrometer enables high throughput and rapid measurements without the need for complex and expensive instrumentations. This would enable the development of low-cost, compact, and rugged devices, suitable for the home-consumer market. The alternative NIR spectroscopic hardware that would provide optical throughput on the same order of magnitude is the Fourier transform spectrometer,[9] which is in fact the more commonly used instrument for experimental work in this field. It is well known, however, that it is significantly more complex mechanically and electronically, and that it requires greater components and subassembly accuracy.

3 Experimental Methods and Data Collection

In this experiment, glucose in 30 human plasma samples from various donors were measured. Glucose spectra were extracted, and the concentrations predicted.

3.1 *Materials*

Plasma samples were purchased from George King Bio-Medical, Incorporated (product number 0070-30). The samples came from 30 different nondiabetic donors. To make high glucose concentrations as found in diabetic patients, anhydrous glucose was added to 19 samples, creating concentrations between 194 mg/dL (10.8 mM) and 571 mg/dL (31.7 mM). The unaltered set contained glucose concentra-

tions between 103 mg/dL (5.7 mM) and 167 mg/dL (9.3 mM). With this dataset, the hypoglycemic limits were not explored. The reference glucose values were measured by a commercial "finger-prick" sensor (Accu-Chek Active™, Roche Diagnostics Corporation, Indianapolis, Indiana). Note that despite the amplification of glucose concentration through the addition of anhydrous glucose, the resulting plasma glucose concentrations are still within what is considered to be the clinically relevant range. Most commercial glucose meters are designed to read blood glucose concentrations up to 600 mg/dL.

3.2 *Spectral Readings*

Each solution was put in a 2-mm pathlength quartz cuvette. Although a shorter pathlength might produce better prediction results due to lower water absorption (and hence better spectral signal-to-noise ratio), the 2-mm pathlength was considered to be the minimum pathlength required to represent actual thin tissue transmission measurement, such as through the webbing tissue between the thumb and the index finger or through the ear lobe. Three absorption spectra were obtained for each solution without removing the sample from the cuvette. Samples were run in random with respect to the glucose concentration. Each absorption spectrum $a(\lambda)$ was obtained by averaging 100 transmission spectra (measurement time of 15 sec) and transforming it logarithmically:

$$a(\lambda) = -\log_{10}\left(\frac{S(\lambda)}{10}\right), \tag{2}$$

where $S(\lambda)$ was the single-beam spectrum measured through the plasma sample. The constant 10 was chosen so that all of the absorption spectra are positive (the maximum detector voltage value was 10). Note that the absorption spectra were essentially logarithmically transformed, single-beam transmission spectra. No repetitive referencing to a background sample (such as background air or water), or sometimes called "instrument baseline recalibration," was performed throughout the experiment. Thus, the success of the experiment also relied on the stability of the system over the experiment period, which was approximately 5 h. The experiment was carried out in a regular photonics laboratory without the use of additional sample or environment control, such as temperature control, humidity control, etc. Note that the denominator of Eq. (2) is commonly a "sample reference" such as a spectrum of background air or water instead of a constant. The use of either a reference spectrum or a constant would yield the same analysis results, as we are always concerned only with spectral variations, not the absolute absorption spectra.

4 Spectral Preprocessing for Baseline Corrections

Spectral preprocessing here refers to the processing of raw absorption spectra $a(\lambda)$ prior to the application of a multivariate algorithm for calibration and prediction. The main purpose of this preprocessing step is to remove or suppress the effects of baseline noise generally caused by sample, instrumental, and/or environmental variations.

Each of the triplicate plasma spectral set produced two difference spectra, $a_{d1}(\lambda)$ and $a_{d2}(\lambda)$, which were the difference spectrum of the first and the second spectra $(a_1 - a_2)$, and the difference spectrum of the first and third spectrum $(a_1 - a_3)$, respectively. This way, 30 plasma samples produced 60 difference spectra. An ideal difference spectrum of such repeat spectra is one with a shape of a flat line at zero across the wavelengths. Actual repeat spectra, however, generally exhibit large baseline noise. An example of such a repeat-spectra difference spectrum can be seen in the top part of Fig. 3. The baseline noise is likely due to slight temperature differences between the samples.[11]

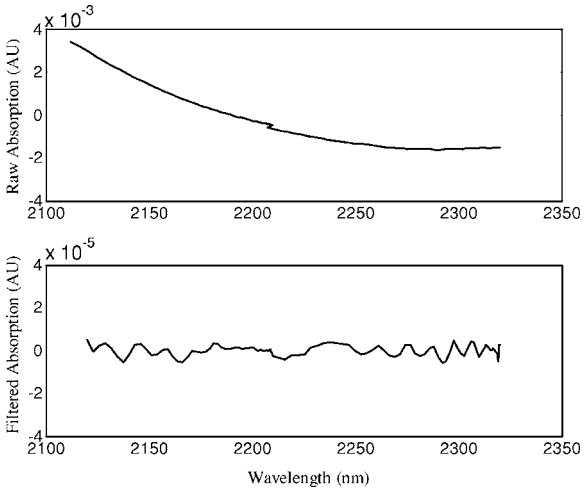

Fig. 3 A typical raw difference spectrum of the repeat spectra (top) and the corresponding filtered spectrum (bottom). The discontinuity at ~2200 nm is due to the transition between the two filters.

The main purpose of the preprocessing algorithm is to remove this baseline noise. However, in this work we extended our effort in the preprocessing algorithm development a step further, that is, to develop an algorithm that was robust, and one that would be applicable to our future work involving highly scattering tissue samples. The subsequent paragraphs report our preliminary work in this aspect.

Spectral variations due to scattering can be described by a single coefficient, called the reduced scattering coefficient μ_s', in units of cm^{-1}.[12] It is suggested that the dependence of the reduced scattering coefficient on wavelength has the following form[13]:

$$\mu_s' = b\lambda^{-p}, \tag{3}$$

where b is a constant and p is the scatter power, which ranges from 1 in the case of Mie scattering and 4 in the case of Rayleigh scattering. For our preprocessing algorithm development purpose, the most significant characteristic of the scattering theory is the fact that when plotted against the wavelength λ, this coefficient would be shaped similar to a baseline noise spectrum. In other words, it has a "slow" dependence on wavelength. This fact has been proven experimentally.[14–17]

Several preprocessing methods were evaluated, which included the polynomial fit, spectral differentiation, and Fourier filtering (or bandpass filtering). The effectiveness of the method was measured by measuring the peak-to-peak magnitudes of the preprocessed difference spectrum. The most ef-

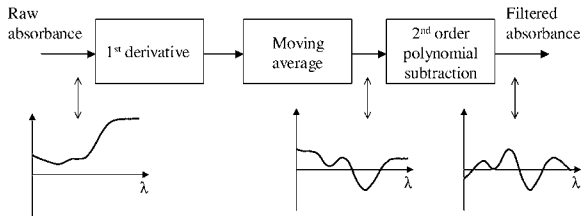

Fig. 4 Schematic and illustration of the spectral preprocessing method to suppress baseline variations.

fective method would lead to difference spectra having the minimum standard deviation from the ideal line at zero across the wavelength axis.

With such a trial and error, a method found most effective was one that used a combination of a first-order differentiation and a second-order polynomial subtraction. For each spectral window obtained by each filter, a first-order spectral differentiation is first applied, in which difference values between two neighboring spectral data points are computed. A moving-average smoothing method is then used to compensate for the decrease in spectral signal-to-noise ratio inherent to spectral differentiations. It involves convolving the spectrum with a certain "window." In this case, the window is a vector 1,1,1,1—a rectangular window with a width of four data points. Finally, a second-order polynomial fit is applied to further suppress the baseline variations, while preserving the relevant molecular absorption features. The spectral preprocessing method is illustrated by the schematic in Fig. 4. The plots underneath the block diagram are example absorbance plots at different stages of the spectral preprocessing algorithm, as indicated by the vertical arrows.

The bottom part of Fig. 3 shows the resulting preprocessed difference spectrum. As seen, the preprocessing algorithm effectively removes the baseline error. The resulting spectral variations compose mainly of the high-frequency detector and/or electronic noise, which is about 3 orders of magnitude lower than the original baseline noise. The baseline noise removed is believed to also include features from water displacement, as water absorption spectrum is featureless within the spectral region considered.

Note that the optimum preprocessing method depends on the spectral range and the data point spacing, which is dependent on the type of the spectrometer used and its wavelength-axis settings. Therefore, our findings in this regard are particular to our instrument, and may not be directly applicable to spectral data obtained by other instruments. We believe that in the particular wavelength region considered, which is relatively narrow, spectral variations due to water displacement and instrumental drifts have been effectively eliminated. Thus, the resulting spectral variations are likely to originate from molecular absorptions that have spectral features in this wavelength region.

By analyzing the preprocessed repeat spectra, we decided to discard two spectral sets out of the original 30. The preprocessed difference spectra from those samples were found to be a couple orders of magnitude higher than the other 28, thus indicating large variations within the sets. We speculated that the unusually large variations were due to formations of air bubbles that we occasionally observed on liquid transfers. As a result, only the remaining 28 samples were used in the subsequent analysis. The 56 repeat spectra from the triplicate plasma samples (28×2) produce noise values in the range between 2.4×10^{-6} and 8.4×10^{-6} AU, with an average value of 5.1×10^{-6} AU. Note that these values are the root mean-square values of the filtered repeat spectra such as the one shown on the bottom part of Fig. 3, between approximately 2120 and 2315 nm.

5 Figures of Merit

In this section, we evaluate the performance of the proposed system for glucose measurements in human plasma through the use of two figures of merit, namely selectivity (SEL) and limit of detection (LOD). These figures of merit are not only applicable to the spectroscopic system described in this work, but can be applied to data obtained by other NIR hardware and software methods.

There are two technical challenges of NIR noninvasive blood glucose measurements, namely the specificity and the sensitivity problems. The specificity problem refers to the challenge of isolating the glucose spectrum from the greatly overlapping spectra of other absorbing and scattering blood and tissue components. The success of isolating the glucose spectrum depends on the uniqueness of its features among the interfering or the background spectra. To gauge this uniqueness, we use a figure of merit, selectivity, which is defined in Sec. 5.1.

The sensitivity problem refers to the challenge of detecting the weak spectral changes associated with physiological variations of glucose in the blood. Resolving 1-mM variation (approximately the level of resolution required for clinically accurate data) in a 1-mm pathlength aqueous solution requires approximately 1 part per 20,000 detection.[9] This is a stringent requirement for any spectroscopic instrument, requiring careful design of the optical, mechanical, electrical, and the software components. To quantify the level of sensitivity achievable, we define a figure of merit, limit of detection, which is defined in Sec. 5.2.

5.1 *Selectivity*

Selectivity (SEL) is a measure of the degree of uniqueness of glucose spectrum in a particular background mixture. It is dependent on the host it is in (plasma, blood, tissue, etc.), as well as on the hardware's spectral resolution and spectral range. It can be quantified by measuring the degree of overlap between glucose spectrum and the background or interfering spectra. To do this, we employ an additional terminology, net analyte signal (NAS).[18–20]

A net analyte signal of a component is defined as the part of its spectrum that is orthogonal to the spectra of the background components. Equivalently, it is orthogonal to the principal components of the background or interference matrix. Essentially, it is the part of the spectrum that is unique to the component. The following paragraphs describe a procedure in obtaining the NAS of glucose in a plasma matrix, and consequently, the SEL.

First, spectra of glucose-free plasma samples are obtained. Assuming absorption linearity, contributions of glucose absorptions to the plasma spectra can be removed if pure-component glucose spectrum is available, and glucose con-

centrations in the plasma samples are known. Given that all these conditions are met, glucose spectra can simply be subtracted out from the plasma spectra:

$$\mathbf{A_{gf}} = \mathbf{A} - \mathbf{c_g a_g^T}, \tag{4}$$

where $\mathbf{A_{gf}}$ is an $m \times n$ matrix containing the glucose-free plasma spectra (m samples and n spectral data points), $\mathbf{A}$ is the $m \times n$ original plasma spectral matrix, $\mathbf{a_g}$ is an $n \times 1$ vector containing the pure-component spectrum of glucose at a unit concentration, and $\mathbf{c_g}$ is an $m \times 1$ vector containing glucose concentration values of the plasma samples.

The next step is the computation of the principal components of the glucose-free plasma spectra. This step is similar to generation of orthogonal basis spectra $\mathbf{V}$ composed of the principal components of a matrix as done in principal component analysis (PCA).[21] $\mathbf{V}$ is an $n \times p$ matrix, where p is the number of principal components used, as chosen by the user. The spectra are mean centered prior to the PCA computation.

Glucose NAS $\mathbf{a_g^*}$ can then be calculated by the following equation:

$$\mathbf{a_g^*} = (\mathbf{I} - \mathbf{V}\mathbf{V^T})\mathbf{a_g}, \tag{5}$$

where $\mathbf{I}$ is an identity matrix. Lorber[18] proposed a method to quantify selectivity SEL, which involves the division of the norm of component NAS by the pure-component spectrum:

$$\mathrm{SEL} = \frac{\|a_g^*\|}{\|a_g\|}, \tag{6}$$

where $\|\cdot\|$ denotes the Euclidean norm. With this method, the selectivity value ranges from zero, which implies a nonselective signal, to one, which implies a fully selective signal. It should be pointed out that the calculated selectivity value will depend on the number of the principal components used to describe the background or interference spectra. A larger number generally decreases the SEL value, as more spectral features are included, thus increasing the chance of overlapping with the glucose spectrum. In general, the number of the principal components used should not be too large, such that the model includes random spectral noise, but large enough to include the important interferences, such as the spectra of protein (albumin and globulin) and triglycerides.

Following the procedure outlined, we obtained glucose NAS and SEL values in the human plasma sample matrix. First, a glucose spectrum was obtained by measuring 500 mg/dL (27.8 mM) of aqueous glucose solution in a 2-mm cuvette. The raw absorption spectrum was then filtered using the preprocessing method discussed in Sec. 4. A filtered water absorption spectrum was subtracted from the glucose spectrum, which was then scaled appropriately to represent a 1-mM glucose spectrum $\mathbf{a_g}$. Note that the highly concentrated glucose solution was used to ensure a high-quality spectrum. Subsequently, the product $\mathbf{a_g}$ and the concentration vector $\mathbf{c_g}$ was subtracted from one of the triplicate plasma spectral datasets $\mathbf{A}$, as described in Eq. (4). Thus, a glucose-free matrix $\mathbf{A_{gf}}$ was constructed. The NAS and SEL values of glucose were then obtained by using Eqs. (5) and (6), respectively.

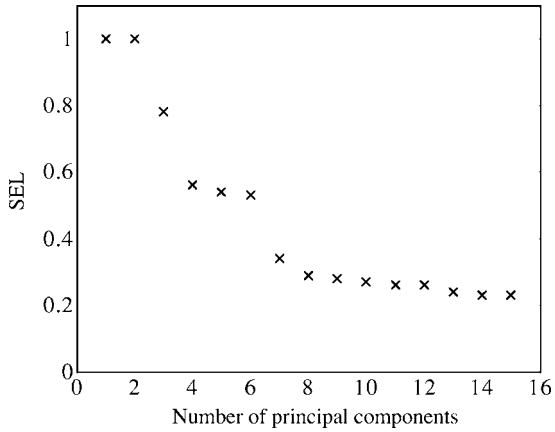

Fig. 5 SEL values of glucose in a plasma matrix as a function of the number of principal components used to model a glucose-free plasma matrix.

Note that repeating the procedure on the other two spectral datasets of the triplicate plasma spectral datasets resulted in similar NAS and SEL values, as expected.

Shown in Fig. 5 are the SEL values as a function of the number of principal components used. Shown in Fig. 6 is glucose NAS with three and four principal components. Note that the spectral features of interest are between approximately 2230 and 2300 nm, encompassing the glucose absorption peak at around 2280 nm. The peak at ~2200 nm does not correspond to any absorption but to the two-filter transition discontinuity. Other peaks or features are considered as noise. As discussed in Sec. 6, four principal components are sufficient to describe spectral variations in the plasma samples. The corresponding SEL value is 0.57. This means that a little over half of the glucose spectrum between 2080 and 2315 nm is unique to glucose in a human plasma matrix.

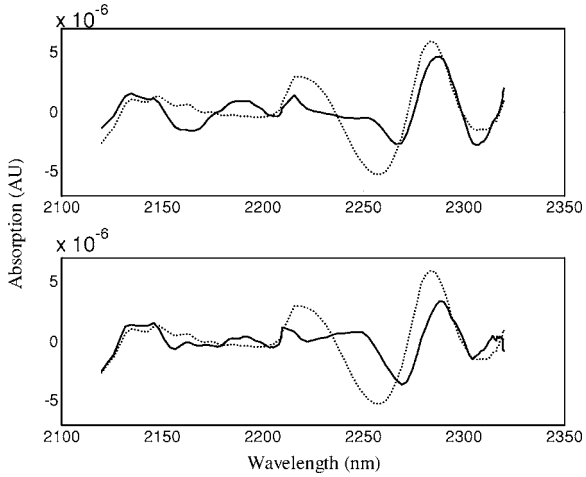

Fig. 6 NAS of glucose (solid lines) in comparison with pure-component aqueous glucose spectrum (dashed lines) for numbers of principal components of 3 (top) and 4 (bottom). The peak at ~2200 nm does not correspond to any absorption but the two-filter transition discontinuity.

5.2 *Limit of Detection*

We wish to estimate the smallest incremental glucose concentration change detectable, called the limit of detection (LOD). This can be done by comparing the magnitude of noise and the magnitude of glucose signal. LOD is estimated to be the concentration level at which the magnitude of glucose signal is "equal" to the noise magnitude. Its definition is similar to the definition of the noise equivalent power (NEP) value, commonly used to quantify the performance of optical detectors, which is simply a comparison between the signal magnitude and the noise magnitude.

In this work, we define the signal to be the peak-to-peak magnitude of the glucose NAS for the band at around 2280 nm, scaled to represent a spectral magnitude from a 1-mM pure-component, aqueous solution in a 2-mm pathlength. As mentioned before, the pathlength of 2 mm is chosen to represent the expected *in vivo* pathlength in measurements through thin tissue, such as the webbing tissue between the thumb and the index finger or through the ear lobe.

To estimate the noise magnitude, we first need to obtain the unmodeled spectral variations or the residual spectra **n** on spectral least-squares fitting using the selected principal components as the basis spectra:

$$\mathbf{n} = \mathbf{x} - \mathbf{c}^{\mathbf{T}}\mathbf{V}^{\mathbf{T}}, \tag{7}$$

where **x** is the background or interference spectrum and $\mathbf{c}^{\mathbf{t}}\mathbf{V}^{\mathbf{T}}$ is the least-squares estimator of **x** using the principal-component matrix $\mathbf{V}^{\mathbf{T}}$. **c** is thus an $n \times 1$ vector of principal component scores obtained by the projection of **x** onto **V**. The following elucidates the process in obtaining the noise spectra: 1. PCA is performed on the glucose-free background matrix, 2. the first k principal components, $\mathbf{V}_1 \ldots \mathbf{V}_\mathbf{k}$ are obtained and stored, 3. a set of i new glucose-free matrix are obtained for analysis (as an independent dataset), 4. classical least-square (CLS) regression is performed on the new matrix using the k principal components as the basis spectra, 5. the residual spectra are obtained and centered about their mean spectrum, and 6. each of the i residual spectra are subtracted by the mean spectrum to obtain the spectral variations. Physically, these spectra represent spectral variations that are not modeled by the hybrid linear analysis (HLA) calibration model (refer to Sec. 6.1 for a description of the HLA method). Thus, they are considered to be the noise or the residuals.

The dotted line in Fig. 7 shows an example of the residual spectrum obtained from the plasma matrix using four principal components (k is equal to 4). The noise magnitude can then be defined to be the average of the rms value of the noise spectra n_{rms}. Note that the noise spectra (and hence the noise value) should be in the same measurement unit as the signal spectra. In this work, for example, all of the measurement spectra are in the absorbance unit (AU).

Having defined the signal and the noise magnitudes, the LOD can then be defined to be:

$$\mathrm{LOD} \approx 3 \times \frac{n_{\mathrm{rms}}}{|a_g^*|_{pk\text{-}pk}}, \tag{8}$$

where $|a_g^*|_{pk\text{-}pk}$ is the peak-to-peak glucose NAS magnitude of 1-mM aqueous glucose. The constant 3 is chosen to compensate for the fact that a rms value of a noise is generally about three times smaller than its peak-to-peak value for a uniformly distributed random noise. Such a multivariate signal-to-noise comparison method and its variations to estimate detection limit have been used widely.[18–20,22,23]

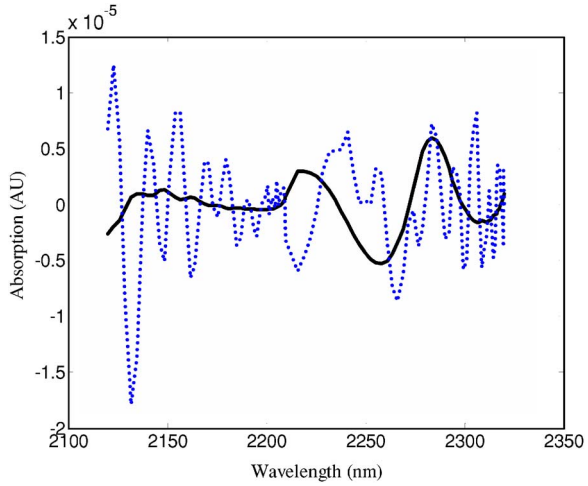

Fig. 7 A residual or noise spectrum of a human plasma matrix on least-squares fitting using 4 principal components (dashed line), and a preprocessed pure-component glucose spectrum scaled to represent 1-mM concentration in a 2-mm pathlength (solid line).

With the procedure outlined earlier and using the first four principal components to model the glucose-free background matrix, the average rms value of the noise spectra is calculated to be 5.2×10^{-6} AU. The peak-to-peak magnitude of the glucose NAS of the band at around 2280 nm is approximately 7.1×10^{-6} AU. Note that these values are obtained from the preprocessed spectra using the combination of a spectral differentiation and a polynomial fit as described Sec. 4. Substituting these values into Eq. (8), the LOD value is estimated to be 2.2. Since a_g^* is scaled in such a way that its magnitude represents the magnitude of 1-mM aqueous glucose absorption, the LOD value of 2.2 means that the detection limit is equal to 2.2 mM (2.2×1 mM). We see later that this value provides a conservative estimate of the glucose standard error of prediction (SEP) values obtained in the glucose-prediction experiment. Note that the LOD values are valid for 2-mm pathlength samples, the pathlength used throughout the experiment.

6 Plasma Glucose Prediction

The 28 samples were divided into a prediction and a calibration set, each containing 14 samples. This was done by first sorting the original samples by their concentrations as measured by the reference method, $c_1, c_2, \ldots, c_{28}$ in increasing value. The odd- and even-numbered samples were then grouped into a prediction and calibration set, respectively. Note that two samples out of the original 30 had been discarded, as explained in Sec. 4.

Two multivariate calibration techniques were used independently. One made use of the NAS of glucose obtained from the calibration sample, which was proposed by Berger, Koo, and Feld,[24] called a hybrid linear analysis (HLA). The second method used was the partial least squares (PLS), the most commonly used multivariate technique in the field.

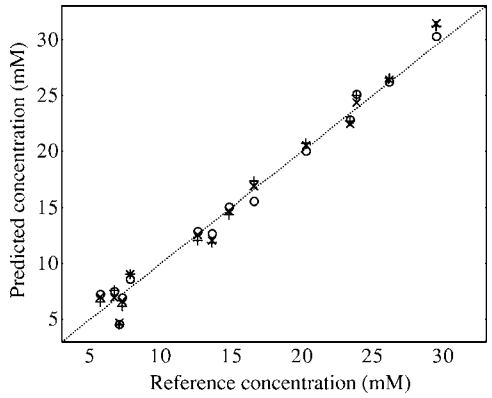

Fig. 8 Glucose prediction plot obtained by a HLA method. ×, +, and ○ represent the first, second, and third dataset, respectively. SEP: 1.14 mM. SER: 0.52 mM. Number of principal components used in the HLA calibration: 4.

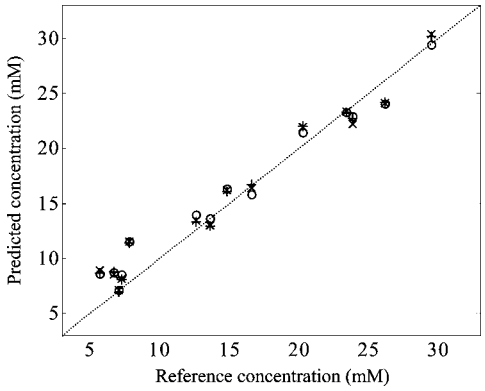

Fig. 9 Glucose prediction plot obtained by a PLS method. ×, +, and ○ represent the first, second, and third dataset, respectively. SEP: 1.45 mM. SER: 0.38 mM. Number of PLS factors: 5.

6.1 *Hybrid Linear Analysis*

The HLA method is a simple and potentially robust method that makes use of the glucose NAS in computing the "unknown" glucose concentrations (the prediction step). This method is potentially more robust than PLS or PCA due to the fact that the calibration model is based on the actual glucose spectrum, rather than on a spectrum obtained through regressions. This eliminates the risks of having a calibration model that is not particular to glucose.

First, glucose NAS $\mathbf{a}_\mathbf{g}^*$ is obtained using Eq. (5). In this case, the orthogonal basis spectra $\mathbf{V}$ are obtained from the glucose-free matrix of the calibration spectral dataset. Glucose NAS is then normalized using the pure-component glucose spectrum:

$$\mathbf{b} = \mathbf{a}_\mathbf{g}^*/(\mathbf{a}_\mathbf{g}^\mathbf{T}\mathbf{a}_\mathbf{g}^*), \tag{9}$$

where $\mathbf{b}$ is the normalized glucose NAS, which is the glucose calibration vector. The predicted glucose concentrations were then obtained by simply multiplying $\mathbf{b}$ and the matrix of the prediction spectral dataset $\mathbf{A}_\mathbf{pred}$:

$$\mathbf{c}_\mathbf{pred} = \mathbf{b}\mathbf{A}_\mathbf{pred}. \tag{10}$$

Figure 8 shows the prediction plot obtained by this multivariate method. The standard error of prediction (SEP) was found to be 1.14 mM, the standard error of calibration (SEC) 2.17 mM, and the standard error of repeatability (SER) 0.52 mM. As the name implies, the SER measures the standard deviation of the concentration difference between the three triplicate readings. Note that whereas SEP value takes into account errors due to reference measurement, liquid transfer/sampling, and spectral measurement, the SER only takes into account errors associated with the spectral measurement.

The number of principal components used to model the interferences is four. Increasing this number beyond four did not improve the SEP values substantially. As mentioned earlier, the general rule is to use the minimum number of principal components that yields acceptable SEP and SER values so as not to overfit the data. In fact, we found that increasing the number of the principal components increased the SER value (while slightly reducing the SEP value), which indicated data overfitting.

6.2 *Partial Least Squares*

The PLS method was used on the same calibration and prediction sets. A similar prediction plot was obtained, shown in Fig. 9. In this case, the SEP, SEC, and SER were found to be 1.45, 1.51, and 0.38 mM, respectively. The number of PLS factors used was five, which was found to yield the minimum SEP value.

In addition to the prediction plot, we also examined the weight loading vectors produced on the PLS calibration step. Haaland and Thomas[25] suggests that the first weight loading vector should contain useful qualitative spectral information, as it represents the first-order approximation to the analyte's pure-component spectrum. As shown in Fig. 10, it remarkably resembles the glucose pure-component spectrum (the top plot is the first PLS loading vector and the bottom plot is the pure-component spectrum of glucose). This finding suggests that the PLS model that was developed and used to compute

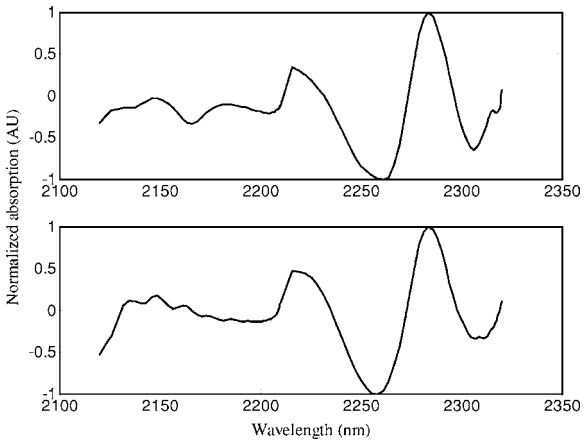

Fig. 10 Upper: PLS first weight loading vector. Lower: pure-component glucose spectrum.

the concentrations in the prediction set was truly particular to glucose, rather than to some secondary factors, thus indicating high-quality measured spectra.

7 Discussions and Conclusions

In this research field, we believe that there are two aspects that require more attention. One concerns the hardware design and the other a better understanding of measured glucose signals. The low-resolution (~10 nm) and narrow-bandwidth (~200 nm) spectral requirements of blood glucose measurements in the long-wave NIR region provide ample opportunities for hardware design optimizations. The most important hardware performance criteria for noninvasive blood glucose measurements are high-throughput and low-noise capabilities. Albeit their high-throughput capability, the commonly used Fourier-transform spectrometers may fail to produce small enough spectral noise values in the near infrared due to their complex design and their high sensitivity to optical misalignments and environmental conditions.[26] The proposed filter-based spectrometer enables high-throughput measurements without the complexity and the sensitivity to environmental disturbances.

One of the major challenges of glucose measurements in a complex biological matrix such as plasma is that the glucose spectrum is greatly overlapped by many interfering spectra. As a result, its qualitative features are difficult to extract and analyze. Empirical-based multivariate calibration techniques are thus heavily relied on, which have the drawback of possibly letting secondary and/or erroneous factors be used in building the glucose calibration vector.

One of our goals in this work is to provide developments or improvements in these two aspects that we see lacking in progress. Details of the hardware design are presented in our previous publication.[9] In this work, we only present brief descriptions of the hardware, which include the modification involving the incorporation of another filter to extend the spectral coverage to cover the whole available combination band regions approximately between 2100 and 2300 nm. Using net analyte signal analysis, we also present methods to quantify selectivity and limit of detection, two most important figures of merit in an effort to understand glucose signal characteristics in complex biological matrices.

Due to the overlapping spectra, a multivariate technique is needed to extract the glucose quantitative information. Most of the works in this field have used the PLS or the PCA techniques. In these cases, glucose calibration vectors are built from empirical data, which may not have obvious relationship with the physical glucose spectrum. Reported in this work is our plasma glucose computation using the net analyte signal-based method—a multivariate technique in which a physical glucose spectrum is used as the calibration vector. This will eliminate the risk of building and using erroneous models that correspond to secondary factors.

We plan to continue this research work by incrementally increasing the complexity of the background matrix to finally measure blood glucose *in vivo*, while ensuring sufficient signal quality at each step.

References

1. C. Fischbacher, K. U. Jagemann, K. Danzer, U. A. Müller, L. Papenkordt, and J. Schüler, "Enhancing calibration models for noninvasive near-infrared spectroscopical blood glucose determination," *Fresenius' J. Anal. Chem.* **359**(1), 78–82 (1997).
2. G. W. Small, M. A. Arnold, and L. A. Marquardt, "Strategies for coupling digital filtering with partial least-squares regression: application to the determination of glucose in plasma by Fourier transform near-infrared spectroscopy," *Anal. Chem.* **65**(22), 3279–3289 (1993).
3. H. M. Heise and A. Bittner, "Multivariate calibration for near-infrared spectroscopic assays of blood substrates in human plasma based on variable selection using PLS-regression vector choices," *Fresenius' J. Anal. Chem.* **362**(1), 141–147 (1998).
4. M. A. Arnold and G. W. Small, "Determination of physiological levels of glucose in an aqueous matrix with digitally filtered Fourier transform near-infrared spectra," *Anal. Chem.* **62**(14), 1457–1464 (1990).
5. U. A. Müller, B. Mertes, C. FischBacher, K. U. Jageman, and K. Danzer, "Noninvasive blood glucose monitoring by means of near infrared spectroscopy: methods for improving the reliability of the calibration models," *Int. J. Artif. Organs* **20**(5), 285–290 (1997).
6. M. J. Mattu, G. W. Small, and M. A. Arnold, "Determination of glucose in a biological matrix by multivariate analysis of multiple bandpass-filtered Fourier transform near-infrared interferograms," *Anal. Chem.* **69**(22), 4695–4702 (1997).
7. N. A. Cingo, G. W. Small, and M. A. Arnold, "Determination of glucose in a synthetic biological matrix with decimated time-domain filtered near-infrared interferogram data," *Vib. Spectrosc.* **23**(1), 103–107 (2000).
8. F. M. Ham, G. M. Cohen, I. Kostanic, and B. R. Gooch, "Multivariate determination of glucose concentrations from optimally filtered frequency-warped NIR spectra of human blood serum," *Physiol. Meas* **17**(1), 1–20 (1996).
9. V. Saptari and K. Youcef-Toumi, "Design of a mechanical-tunable filter spectrometer for noninvasive glucose measurement," *Appl. Opt.* **43**(13), 2680–2688 (2004).
10. V. A. Saptari and K. Youcef-Toumi, "Sensitivity analysis of near infrared glucose absorption signals: toward noninvasive blood glucose sensing," *Proc. SPIE* **4163**, 45–54 (2000).
11. K. H. Hazen, M. A. Arnold, and G. W. Small, "Temperature-insensitive near-infrared spectroscopic measurement of glucose in aqueous solutions," *Appl. Spectrosc.* **48**(4), 477–483 (1994).
12. B. C. Wilson and S. L. Jacques, "Optical reflectance and transmittance of tissues: principles and applications," *IEEE J. Quantum Electron.* **26**(12), 2186–2199 (1990).
13. A. E. Cerussi, A. J. Berger, F. Bevilacqua, N. Shah, D. Jakubowski, J. Butler, R. F. Holcombe, and B. J. Tromberg, "Sources of absorption and scattering contrast for near-infrared optical mammography," *Acad. Radiol.* **8**(3), 211–218 (2001).
14. J. M. Schmitt and G. Kumar, "Spectral distortions in near-infrared spectroscopy of turbid material," *Appl. Spectrosc.* **50**(8), 1066–1073 (1996).
15. G. Marquez, L. V. Wang, S. Lin, J. A. Schwartz, and S. L. Thomsen, "Anosotropy in the absorption and scattering spectra of chicken breast tissue," *Appl. Opt.* **37**(4), 798–804 (1998).
16. T. H. Pham, F. Bevilacqua, T. Spott, J. S. Dam, B. J. Tromberg, and S. Anderson-Engels, "Quantifying the absorption and reduced scattering coefficients of tissue-like turbid media over a broad spectral range with noncontact Fourier-transform hyperspectral imaging," *Appl. Opt.* **39**(34), 6487–6497 (2000).
17. T. L. Troy and S. N. Thennadil, "Optical properties of human skin in the near infrared wavelength range of 1000 to 2200 nm," *J. Biomed. Opt.* **6**(2), 167–176 (2001).
18. A. Lorber, "Error propagation and figures of merit for quantitation by solving matrix equations," *Anal. Chem.* **58**(6), 1167–1172 (1986).
19. J. F. R. Boquè, B. Fernàndez-Band, M. S. Larrechi, and F. X. Rius, "Figures of merit in multivariate calibration. Determination four pesticides in water by flow injection analysis and spectrophotometric detection," *Anal. Chim. Acta* **348**, 167–175 (1997).
20. N. R. Marsili, M. S. Sobrero, and H. C. Goicoechea, "Spectrophotometric determination of sorbic and benzoic acids in fruit juices by a net analyte signal-based method with selection of the wavelength range to avoid non-modelled interferences," *Anal. Bioanal. Chem.* **376**(2), 126–133 (2003).
21. D. L. Massart, B. G. M. Vandeginste, S. N. Deming, Y. Michotte, and

L. Kaufman, *Chemometrics: A Text Book*, Elsevier Science Publishers B. V., Amsterdam (1988).
22. J. F. R. Boquè and F. X. Rius, "Multivariate detection limits estimators," *Chemom. Intell. Lab. Syst.* **32**(1), 11–23 (1996).
23. J. Ferre and N. M. Faber, "Net analyte signal calculation for multivariate calibration," *Chemom. Intell. Lab. Syst.* **69**(1–2), 123–136 (2003).
24. A. J. Berger, T. W. Koo, and M. S. Feld, "An enhanced algorithm for linear multivariate calibration," *Anal. Chem.* **70**(3), 623–627 (1998).
25. D. M. Haaland and E. V. Thomas, "Partial least-squares methods for spectral analysis. 1. Relation to other quantitative calibration methods and the extraction of qualitative information," *Anal. Chem.* **60**(11), 1193–1202 (1988).
26. V. A. Saptari, *Fourier Transform Spectroscopy Instrumentation Engineering*, SPIE Press, Bellingham, WA (2003).